2001

Baryons in the warm-hot intergalactic medium

R Dave

R Cen

JP Ostriker

GL Bryan

L Hernquist

See next page for additional authors

Recommended Citation

Dave, R; Cen, R; Ostriker, JP; Bryan, GL; Hernquist, L; Katz, N; Weinberg, DH; Norman, ML; and O'Shea, B, "Baryons in the warm-hot intergalactic medium" (2001). *ASTROPHYSICAL JOURNAL*. 355.
10.1086/320548

Draft version February 1, 2008
Preprint typeset using LaTeX style emulateapj v. 04/03/99

BARYONS IN THE WARM-HOT INTERGALACTIC MEDIUM

Romeel Davé[1,2], Renyue Cen[1], Jeremiah P. Ostriker[1], Greg L. Bryan[3,4], Lars Hernquist[5], Neal Katz[6], David H. Weinberg[7], Michael L. Norman[8], and Brian O'Shea[8]

Draft version February 1, 2008

ABSTRACT

Approximately $30-40\%$ of all baryons in the present day universe reside in a warm-hot intergalactic medium (WHIM), with temperatures between $10^5 < T < 10^7$ K. This is a generic prediction from six hydrodynamic simulations of currently favored structure formation models having a wide variety of numerical methods, input physics, volumes, and spatial resolutions. Most of these warm-hot baryons reside in diffuse large-scale structures with a median overdensity around $10-30$, not in virialized objects such as galaxy groups or galactic halos. The evolution of the WHIM is primarily driven by shock heating from gravitational perturbations breaking on mildly nonlinear, non-equilibrium structures such as filaments. Supernova feedback energy and radiative cooling play lesser roles in its evolution. WHIM gas is consistent with observations of the 0.25 keV X-ray background without being significantly heated by non-gravitational processes because the emitting gas is very diffuse. Our results confirm and extend previous work by Cen & Ostriker and Davé et al.

Subject headings: Cosmology: observations, large scale structure of Universe, intergalactic medium

1. INTRODUCTION

Observations indicate that most of the baryonic matter in the universe does not reside in galaxies. At high redshifts ($z \gtrsim 2$), the overwhelming majority of baryons are in a diffuse, photoionized intergalactic medium (IGM), observable as H I absorption lines in the spectra of distant quasars (Cen et al. 1994; Zhang, Anninos, & Norman 1995; Miralda-Escudé et al. 1996; Hernquist et al. 1996). The baryonic density inferred from these observations (Rauch et al. 1997) is in good agreement with nucleosynthesis arguments based on observed deuterium abundances (Tytler, Fan, & Burles 1996). But by redshift zero the total baryonic component, inferred from H I absorption, gas and stars in galaxies, and other observations, has declined to a level small compared to that seen at high redshift and expectations from nucleosynthesis (Fukugita, Hogan & Peebles 1998; Hogan 1999). Thus the question arises, where are the baryons at the present epoch?

By the current epoch, hierarchical structure formation has produced deep potential wells into which the baryons accrete, thereby moving a significant portion of the baryons from the IGM into stars, galaxies, groups, and clusters. These complex evolutionary processes may now be modeled directly using cosmological hydrodynamic simulations, enabling an investigation into the location and phase of baryonic constituents in the present-day universe, and suggesting possible avenues for their direct detection.

These hydrodynamic simulations of structure formation indicate that baryons in the universe reside in four broad phases, defined by their overdensity $\delta \equiv \rho/\bar{\rho} - 1$ (where $\bar{\rho}$ is the mean baryonic density) and temperature T:

1. *Diffuse:* $\delta < 1000$, $T < 10^5$ K. Photoionized intergalactic gas that gives rise to Lyman alpha absorption.

2. *Condensed:* $\delta > 1000$, $T < 10^5$ K. Stars and cool galactic gas.

3. *Hot:* $T > 10^7$ K. Gas in galaxy clusters and large groups.

4. *Warm-Hot:* $10^5 < T < 10^7$ K. The "Warm-Hot Intergalactic Medium" (WHIM), discussed here.

.

Cen & Ostriker (1999; hereafter CO99) and Davé et al. (1999; hereafter DHKW) predicted that a sizeable fraction of all baryons at the present epoch reside in this last warm-hot phase (see Figure 2 of CO99 and Figure 12 of DHKW). Such a reservoir has significant implications for producing an accurate census of baryons for comparison with nucleosynthesis arguments (e.g. Fukugita, Hogan & Peebles 1998) because gas at these temperatures and densities is difficult to detect in either absorption or emission, as we will discuss in §6.

In this paper we study the nature and evolution of warm-hot gas in a ΛCDM universe, using a suite of cosmological hydrodynamic simulations having a wide range of numerical and physical parameters. The purpose of this paper is to ask how robust simulation predictions are to

[1]Princeton University Observatory, Princeton, NJ 08544; rad,cen,jpo@astro.princeton.edu
[2]Spitzer Fellow
[3]Department of Physics, Massachusetts Institute of Technology, Cambridge, MA 02139; gbryan@alcrux.mit.edu
[4]Hubble Fellow
[5]Harvard-Smithsonian Center for Astrophysics, Cambridge, MA 02138; lars@cfa.harvard.edu
[6]Department of Astronomy, University of Massachusetts, Amherst, MA, 01003; nsk@kaka.phast.umass.edu
[7]Department of Astronomy, Ohio State University, Columbus, OH, 43210, dhw@astronomy.ohio-state.edu
[8]Astronomy Department, University of Illinois at Urbana-Champaign, Urbana, IL 61801; norman,bwoshea@ncsa.uiuc.edu

TABLE 1
SIMULATION PARAMETERS.

	Code	Ω	Ω_Λ	n	Ω_b	H_0	σ_8	L [a]	ϵ [b]	$m_{\rm bar}$ [c]	Physics [d]	$\frac{\Omega_{\rm WHIM}}{\Omega_b}$	$C_{\rm WHIM}$ [e]
D1	PTreeSPH	0.4	0.6	0.95	0.0473	65	0.8	50	7	8.5×10^8	1,3,4	0.30	244
D2	PTreeSPH	0.4	0.6	0.95	0.0473	65	0.8	11.11	3.5	1.1×10^8	1,3,4	0.29	405
C1	TVD-PM	0.37	0.63	0.95	0.049	70	0.8	100	200	1.6×10^8	1,2,3,4	0.42	34
C2	TVD-PM	0.37	0.63	0.95	0.049	70	0.8	50	100	2.0×10^7	1,2,3,4	0.37	106
B1	AMR	0.3	0.7	1.0	0.04	67	0.9	100	50	7.9×10^9	adiabatic	0.32	208
B2	AMR	0.3	0.7	1.0	0.04	67	0.9	100	1	9.9×10^8	1,2,3,4	$\approx 0.3^\dagger$	$\approx 400^\dagger$

[a]Box size in comoving h^{-1}Mpc.

[b]Spatial resolution in comoving h^{-1}kpc; for PTreeSPH and AMR, this is the highest resolution achieved in dense regions.

[c]Baryonic mass resolution in $M_\odot$. In TVD-PM, this is the average mass per cell.

[d]1 ≡ H, He cooling; 2 ≡ Metal cooling; 3 ≡ Photoionization; 4 ≡ Star formation & feedback.

[e]Clumping factor of warm-hot gas at $z = 0$; see §5.

[†]Values extrapolated from $z = 0.75$ to $z = 0$ based on a comparison with simulation B1.

these parameters, to examine the physical state of warm-hot gas in the universe, and to investigate constraints on warm-hot gas from soft X-ray background observations.

In §2 we briefly describe the simulations used. The evolution of diffuse gas at high redshift into condensed, hot, and WHIM gas at the present epoch is quantified in §3. Our primary result, presented in §4, is that the WHIM accounts for a significant fraction ($\sim 30 - 40\%$) of baryonic mass at $z = 0$, regardless of variations in spatial resolution, input physics, or hydrodynamic algorithm. This is because the evolution of the WHIM is driven primarily by shock-heating of gas falling into gravitationally-generated potential wells, a process which is well-understood and modeled, and only secondarily by processes such as supernova feedback, radiative cooling, and photoionization. Furthermore, most of the WHIM gas is at relatively low overdensities, so shock heating of intergalactic gas occurs during flows onto non-equilibrium large-scale structures such as filaments. The majority of warm-hot gas is found outside of virialized objects such as galactic halos and galaxy groups. The low overdensities explain why radiative cooling and supernova heating do not drive its evolution, and why the presence of this component probably does not violate constraints from the X-ray background, as we show in §5. Finally, we briefly discuss strategies for direct detection of this gas, noting that the easiest place to detect emission from WHIM gas is relatively close to galaxies, where it is dense, even though most of the warm-hot baryons are not in these regions. In summary, the WHIM is a robust and generic prediction of currently popular hierarchical structure formation models, and it contains roughly one-third of all baryons in the universe today.

2. SIMULATIONS

We use six cosmological hydrodynamic simulations of randomly-selected volumes in Λ-dominated Cold Dark Matter universes, employing three different numerical techniques, with a range of physical and numerical parameters. These parameters are summarized in Table 1. Simulations run with Parallel TreeSPH (Davé, Dubinski & Hernquist 1997) are labeled D1 and D2, simulations run with TVD-PM (Ryu et al. 1993) are labeled C1 and C2, and simulations using Adaptive Mesh Refinement (AMR; Bryan 1999) are labeled B1 and B2. The cosmology chosen is close to the "concordance model" which is in agreement with a wide variety of observations (Bahcall et al. 1999).

For our purposes, the significant inputs are the variations in spatial resolution ($1 \rightarrow 200h^{-1}$kpc), baryonic mass resolution ($2 \times 10^7 \rightarrow 10^9 M_\odot$), boxsize ($11.11 \rightarrow 100\ h^{-1}$Mpc), input physics, and hydrodynamic algorithms. D1 and D2 are high spatial resolution Lagrangian (particle-based) simulations, C1 and C2 are lower spatial resolution Eulerian simulations having high mass resolution and employing the Total Variation Diminishing scheme, and B1 and B2 are high resolution adaptive mesh simulations based on the Piecewise Parabolic Method (note the exceptional resolution of $\sim 1h^{-1}$kpc achieved by AMR in the high density regions). All simulations except B1 include radiative cooling from H and He, photoionization heating, and star formation; B1 includes none of these. C1, C2, and B2 additionally include metal-line cooling, with the metallicity determined self-consistently from supernova output. All simulations use a Λ-dominated cold dark matter universe, having similar power at cluster and galaxy scales. B2 has only been evolved to $z = 0.75$, but this will be sufficient to indicate the relevant trends.

3. EVOLUTION OF INTERGALACTIC GAS

Figure 1 shows the evolution of the baryonic mass fraction in the four phases described above. The four panels show results from simulations D1, D2, C1 and C2. Despite differences in simulation volume, resolution, and numerical method, the evolution of various phases is qualitatively similar. At high redshift ($z \gtrsim 2$), the dominant fraction of baryons resides in diffuse gas (dashed lines) giving rise to Lyman alpha forest absorbers, as has been explored in detail elsewhere (see Rauch 1998 for a review). As structure forms, diffuse gas is shock-heated, producing warm-hot gas (solid lines). Gas that is driven to higher densi-

ties due to gravitational instability is able to cool into the condensed phase (dotted lines) and form stars. At lower redshifts ($z \lesssim 2$), large potential wells are produced that shock-heat gas to $T > 10^7$ K, giving rise to hot cluster gas (dot-dashed curves). Nevertheless, at the present epoch, the total fraction of baryons in clusters is small.

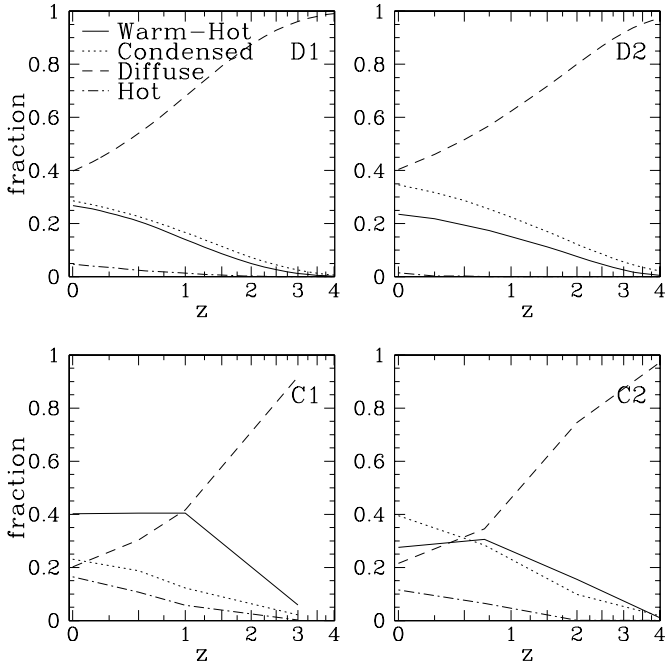

Figure 1: Evolution of mass fractions in four baryonic phases, in four simulations.

Figure 1 shows that the fraction of diffuse baryons at the present epoch is between 20% and 40%, the fraction of warm-hot baryons is $30-40\%$. Gravitationally bound baryons, i.e. those in stars, galactic gas, clusters, and intragroup media, make up the rest. Thus baryons in the present-day universe are divided roughly equally among diffuse, warm-hot, and bound components.

While all the simulations are qualitatively similar, the exact distribution of gas in these phases is sensitive to details of the simulations. For instance, the condensed phase fraction is sensitive to how gas cools and forms stars in these simulations, which in turn is significantly affected by resolution (since cooling and star formation $\propto \rho^2$). Also, the effect of supernova feedback heating depends strongly on resolution, as we will discuss later. The growth of structure is affected by the amount of large-scale power present. In particular, the hot gas fraction in clusters is sensitive to cosmic variance, since it is dominated by the largest virialized objects in the volume. Other phases, including the warm-hot phase, are less sensitive to volume effects, as we show in §4.1.

All things considered, it is not surprising that there are differences up to a factor of two in the fractions in various phases at $z = 0$. While the differences may be significant, an investigation of their exact causes is beyond the scope of this work, though these differences offer clues into the physical processes driving WHIM evolution, as we will explore in §4.1. Rather, we focus on the remarkable qualitative consistency in the evolution of various gas phases, given the variety of simulation methodologies utilized.

For the condensed phase, a census of baryons in stars and cold gas estimates its mass fraction to be around 20% (Fukugita, Hogan & Peebles 1998). The simulations shown generally produce somewhat higher values for the condensed fraction, but there are uncertainties in the contributions from low-mass stars and supernova remnants. Of these simulations, C2 contains the largest fraction of condensed gas ($\sim 40\%$), while the rest are all lower, down to $\sim 25\%$ for simulation C1. B1, of course, has virtually no condensed gas since it does not include cooling. In what follows, we will fix the condensed fraction to be 20% and redistribute the excess condensed gas equally among all the other components, assigning a somewhat arbitrary fraction of 1/3 of it to the WHIM (the only component we examine from here on), in order to facilitate a less resolution-dependent comparison of the intergalactic components in these simulations.

4. THE WARM-HOT INTERGALACTIC MEDIUM

4.1. *Evolution of* $\Omega_{\rm WHIM}$

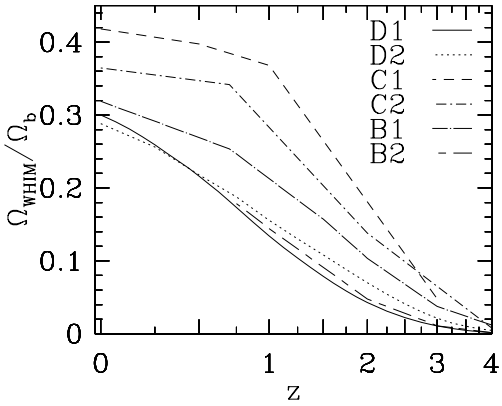

Figure 2: Evolution of $\Omega_{\rm WHIM}$ in our six simulations. For this comparison, the baryonic fraction in cold galactic gas and stars has been fixed at 20% in all simulations.

Figure 2 shows the evolution of the mass fraction of baryons in warm-hot gas, $\Omega_{\rm WHIM}/\Omega_b$, for our six simulations, with the condensed component having been fixed at 20%. C1 and C2 have the highest WHIM fractions, at 42% and 35% of baryonic mass, respectively, at $z = 0$. D1 and D2 have lower WHIM fractions at the present epoch, around $\sim 30\%$. B2 has only been evolved to $z = 0.75$, but its evolution closely mirrors that of the Lagrangian runs, so we expect its WHIM fraction will also be $\sim 30\%$ by $z = 0$. These values are listed in Table 1. By the present epoch, all simulations have WHIM fractions within 50% of each other. Simulation B1 does not include radiative cooling, so it is an unphysical model that will only be used for comparison with B2.

We expect that the evolution of warm-hot gas is governed by shock heating of intergalactic gas onto large-scale structure, supernova feedback, and radiative cooling. Numerical considerations such as resolution, volume and hydrodynamic algorithm may also play a role. In this section we use case-by-case comparisons among our six simulations to examine how each of these processes affects WHIM evolution in our models.

All of our simulations explicitly include the growth of structures and the accretion of gas onto those structures. The qualitative consistency of WHIM evolution in all our

simulations, including simulation B1 without cooling or star formation, suggests that gravitational shock heating of gas falling on large-scale structures is the dominant heating mechanism for WHIM gas. This is an important point, as it suggests that all other differences between these simulations are of secondary importance.

The most obvious differences between models are that D1, D2 and B2 all predict similar WHIM evolution, while C1 and C2 have more WHIM gas. The primary distinction between these sets of simulations is spatial resolution. This manifests itself in various ways, as it affects gas cooling, the rate at which stars form, and the the injection of supernova heat energy into intergalactic gas. To elaborate on this last point, high-resolution runs (D1, D2, B2) deposit feedback energy (thermal only) locally in very high density regions where stars are forming, and thus it quickly radiates away, with virtually none of it being distributed into the intergalactic medium. Conversely, lower-resolution runs (C1 and C2) deposit the same supernova energy over hundreds of kiloparsecs, resulting in a significant fraction of feedback energy escaping into diffuse regions where it cannot radiatively cool away. None of the simulations here are capable of resolving supernova-driven galactic winds through a multi-phase interstellar medium, which are likely to be responsible for distributing energy and metals into the diffuse IGM (Mac Low 2000; Efstathiou 2000), thus we are relying on heuristic modeling of these processes. As we discuss in §4.2, it is in the distribution of feedback energy where resolution plays its most crucial role in predicting the evolution of WHIM gas.

First we examine the effect of radiative cooling. Simulation B1 has no cooling, whereas simulation B2 is a similar run with cooling (and is our highest spatial resolution run). Cooling has a greater effect at earlier times because intergalactic gas is denser then and thus can cool significantly. After $z \sim 3$, the rate of growth of the WHIM fraction is similar in B1 and B2, suggesting that WHIM gas is no longer affected by cooling. Even by $z = 0.75$, the difference between B1 and B2 is not large, indicating that cooling plays a minor role in the overall evolution of WHIM gas.

Eulerian codes resolve shock fronts better than SPH in diffuse regions (Kang et al. 1994), because they have a higher density of resolution elements there, and, in the case of the Eulerian codes discussed here, because they incorporate explicit shock capturing algorithms to resolve fronts over two cells. If a significant component of shock heating arises from small-scale shocks unresolved by SPH, Eulerian codes may produce higher temperatures. One might suspect that the difference between PTreeSPH runs and TVD-PM runs could be partially due to this effect. However, B2 is also an Eulerian simulation, yet it has nearly the same WHIM fraction as the Lagrangian runs. So this cannot be a significant effect.

Simulation volume could also play a role in the amount of WHIM gas, since larger volumes contain larger perturbations that can result in stronger gravitational shock heating. This may explain the difference between C1 and C2, whose box lengths differ by a factor of two. However, D1 has a box length five times that of D2, yet their WHIM fractions are nearly identical at all times. Furthermore, B2 has twice the box length of D1, yet its WHIM fraction is in good agreement with D1 and D2. As we will show in the next section, typical WHIM gas is at very moderate overdensities, and cosmic variance in that regime is typically small, in contrast to the hot IGM fraction which is dominated by rare, massive objects (i.e. clusters) whose numbers are more sensitive to simulation volume.

It is possible that opposing effects are causing D1, D2 and B2 to be similar. For instance, D1 resolves shock fronts better than D2, perhaps resulting in more shock heating and making up for its lack of large-scale power. It is also possible that the adaptive refinement of B2 results in more cooling in shock fronts, compensating for its larger volume. However, unless all of these effects are of secondary importance, cancellations at the level we find here would require a remarkable coincidence.

The parameters of the underlying cosmological model are expected to have a non-negligible effect on the WHIM component. The rate of structure evolution in large part determines how much shock-heated gas is present at any epoch. While we have not sampled a range of cosmologies here, DHKW examined four cosmologies, namely ΛCDM, Tilted CDM, Cold+Hot DM, and Open CDM models, using numerical parameters similar to those of simulation D2. The differences between the WHIM fractions (called "shocked" gas in DHKW) in those models at the current epoch is comparable to the differences seen here due to other factors, as indicated by their Figure 12. Similarly, CO99 examined ΛCDM, Cold+Hot DM, and Open CDM models, and also found broad consistency. Thus while our quoted fractions may be specifically for a ΛCDM cosmology, our qualitative conclusions are unlikely to be highly sensitive to cosmology.

In summary, the evolution of $\Omega_{\rm WHIM}$ is qualitatively consistent among all simulations examined, and results in $\approx 30 - 40\%$ of baryons residing in the WHIM today. Radiative cooling, simulation volume, and algorithmic details do not significantly affect WHIM evolution in these runs.

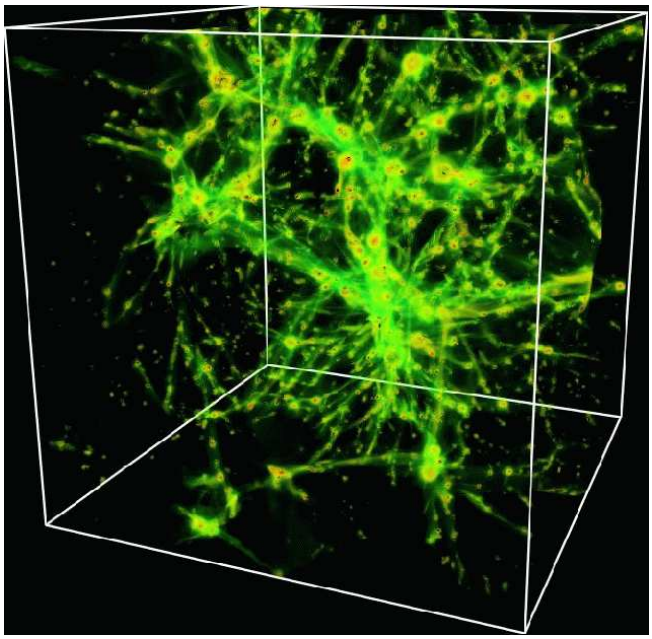

Figure 3: WHIM gas in simulation C2. Contours are color coded by overdensity; green represents overdensity $\delta \sim 10$, while red shows $\delta \sim 10^4$.

4.2. *The Physics of WHIM Gas*

We now explore the physics that drives the formation and evolution of WHIM gas. A qualitative physical picture of WHIM gas may be obtained by examining Figure 3, which shows the location of gas in simulation C2 having $10^5 < T < 10^7$K, with contours color-coded by density. WHIM gas is seen to primarily trace out filamentary large-scale structures. Like the intergalactic medium, WHIM gas does cluster around dense regions that are sites of galaxy formation. However, we will show below that the majority of WHIM gas is contained in the filaments.

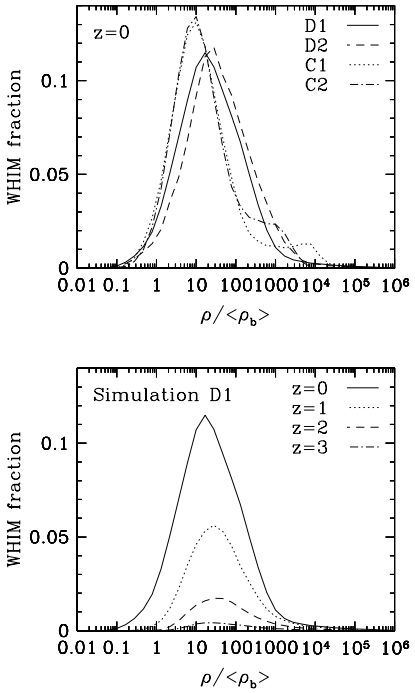

Figure 4: Top panel shows the mass fraction of WHIM gas as a function of density at $z = 0$ in our simulations. Bottom panel shows the same quantity at $z = 0, 1, 2, 3$ in simulation D1.

The top panel of Figure 4 quantifies the spatial distribution of WHIM gas in the universe. It shows a histogram of WHIM gas mass as a function of density, for simulations D1, D2, C1, and C2. All four simulations consistently show that the dominant fraction of WHIM gas is at relatively low densities, with a peak around an overdensity of $\sim 10 - 30$. Simulations B1 and B2 are not shown because B1 does not include cooling and B2 has only been evolved to $z = 0.75$. Still, B1 at $z = 0$ and B2 at $z = 0.75$ show peak overdensities of 18 and 21, respectively, so they are consistent with the other simulations. $70 - 80\%$ of WHIM baryons lie in the overdensity range $5 < \delta < 200$, typical of filaments.

The typical overdensities of WHIM gas are much smaller than that of matter contained in bound, virialized objects. A maximal estimate of the bound fraction of WHIM gas may be obtained as the fraction of WHIM gas with $\delta \gtrsim 60$, which is approximately the overdensity at the virial radius of an isothermal sphere in a ΛCDM cosmology. The mass fraction of WHIM gas with $\delta \gtrsim 60$ is $\approx 30\%$ in our simulations. Clearly some of this gas will not be bound, but rather infalling material. As an independent check, we use the group finding algorithm SKID[1] (Spline Kernel Interpolative DENMAX) to identify bound warm-hot particles in simulation D1, and find a bound fraction of WHIM gas between $\sim 10\%$ and $\sim 25\%$, depending on the linking length used ($50 - 500h^{-1}$kpc). The lower end of this range probably corresponds to gas contained in galactic halos, although the extent of a galactic halo becomes ill-defined when it resides within a group or cluster. In summary, WHIM gas is mostly an intergalactic component, with a majority of it residing outside of virialized structures such as galaxies or groups. Note that coronal gas in galaxies also lies in the warm-hot temperature range, but it is a very small fraction of the galactic baryonic mass, as most galactic baryons are tied up in stars and cold gas.

How can intergalactic gas be heated to $T > 10^5$ K without being bound in a massive virialized halo? One way would be if energy was added from non-thermal processes such as supernova feedback. However, this is not the driving process for WHIM gas in these simulations. Supernova feedback energy is added in all simulations shown in Figure 4, but in simulations D1, D2 and B2 the effect is negligible, since, as discussed before, feedback is added purely thermally into very dense regions, where it radiates away almost immediately and adds no heat to diffuse regions. But even in these high-resolution simulations, where supernovae add negligible heat to WHIM gas, the typical overdensities are smaller than those typical of virialized halos.

Supernova heating is, however, likely to be responsible for the somewhat lower overdensities in simulations C1 and C2 as compared to the higher resolution simulations, so its effect is non-negligible. The differences cannot be due to other spatial resolution effects such as cooling, as C1 and C2 are themselves quite similar, as are D1 and D2. Instead, the lower spatial resolution in C1 and C2 results in significant supernova energy being deposited in intergalactic gas, as described in the previous section. This additional feedback heating raises the pressure of intergalactic gas and lowers the typical density. Furthermore, because supernova energy is not radiated away immediately, there is a small component of warm-hot gas in and around galaxies seen as the high-density bump for C1 and C2 in Figure 4. Note that the densities in D1 and D2 are computed slightly differently than in C1 and C2; in the former, Lagrangian runs, the density field is smoothed by the (variable) smoothing length of the particle, while in the Eulerian runs the smoothing is fixed at the cell size. However, since in both cases the smoothing is done on scales smaller than the density variations, this is not expected to produce any systematic differences in the resulting densities.

The effect of supernova heating can be roughly estimated by the following simple argument. Consider two extreme cases, one where all supernova energy is deposited within dense regions where it immediately radiates away, and another where supernova energy is distributed uniformly over all baryons in the universe. The former case is a reasonable approximation for the Lagrangian runs D1 and D2 as well as the high-resolution AMR run B2, while the latter is closer to the Eulerian runs C1 and C2 (though

[1] http://www-hpcc.astro.washington.edu/TSEGA/tools/skid.html

clearly a much more extreme case). In the former case, supernovae add no heat to WHIM gas. In the latter, the specific heat added per baryon yields a temperature increase of

$$\delta T_{\rm SN} = \frac{\Omega_* \, \rho_{\rm crit} \, \epsilon_{\rm SN}}{k_B \, \bar{n}_H}, \qquad (1)$$

where Ω_* is the cosmic mass fraction in stars, $\rho_{\rm crit}$ is the critical density, $\epsilon_{\rm SN}$ is the specific energy output per unit mass of stars formed, and $\bar{n}_H$ is the mean number density of H atoms. We take $\Omega_* = 0.1\Omega_b = 0.002h^{-2}$, and $\epsilon_{\rm SN} = 2.5 \times 10^{48}$ erg g$^{-1}M_\odot$ from a Salpeter IMF with each supernova from a star with $M > 8M_\odot$ outputting 10^{51} ergs. Then, $\delta T_{\rm SN} = 0.2$ keV $\approx 2 \times 10^6$ K. Assuming isentropic heat distribution, $\rho T^{\frac{3}{2}} =$ constant, so gas with $T \approx 4 \times 10^6$ K (the maximum of the temperature distribution, as we will show in Figure 5) will have its density reduced by roughly a factor of two compared to the no heating case. This is roughly the level of reduction seen in the Eulerian as compared to the Lagrangian runs. Clearly this model is overly simplistic, as it would predict that all intergalactic gas has $T \gtrsim 10^6$ K, but it does roughly indicate the magnitude of the effect of supernova heating.

Note that there are no other heating processes in these simulations that contribute significantly to the WHIM. For instance, photoionization only heats gas to $\sim 10^4$ K. Any other heating process one could devise, such as cosmic rays or supernovae occuring in dwarf galaxies in voids, would add more pressure support to the gas, and thus would push the typical density of WHIM gas even lower. Thus our simulations indicate that WHIM gas is heated to $T > 10^5$ K primarily by shock-heating of gas accreting onto large-scale structure. These structures, typically filamentary, are *not* virialized or in dynamical equilibrium.

In the previous section we showed empirically that radiative cooling has a minor effect on WHIM evolution. This may be understood physically given that warm-hot gas is typically at such low overdensities that it cannot collapse into virialized objects, and due to the metagalactic photoionizing background most intergalactic gas lies well within the optically thin regime (see DHKW, Figure 10). Thus typical WHIM gas is too diffuse to self-gravitate or self-shield, and has no way to achieve the densities required to make radiative processes important. Improving the numerical resolution of our simulations would not change this result, as it is based on simple physical arguments.

The bottom panel of Figure 4 shows a histogram of WHIM gas mass for the D1 model at $z = 0, 1, 2, 3$ (solid, dotted, dashed, long dashed lines). There is a slight trend to higher overdensities at earlier times, since at early times the contribution from virialized structures is greater. This is because gas has not had time to accrete and shock on more diffuse structures, and the largest structures at earlier times have lower temperatures that can fall into the warm-hot range. Still, this is a minor effect; basically, the peak overdensity does not evolve significantly with redshift.

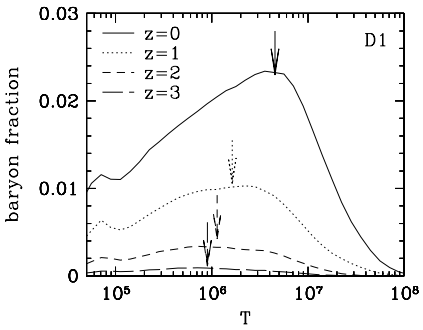

Figure 5: The mass fraction of baryons as a function of temperature in simulation D1, at $z = 0$ (solid), $z = 1$ (dotted), $z = 2$ (short dashed) and $z = 3$ (long dashed). The arrows indicate the predicted peak temperature from gravitational shock heating at various z, from equation 2.

Figure 5 shows the temperature distribution of intergalactic gas with $T > 10^{4.5}$ K in simulation D1 at $z = 0, 1, 2, 3$. The amount of gas at these warm-hot and hot temperatures grows with time, as seen from Figures 1 and 2. The temperature at the peak of the distribution grows in time as well, reflecting the fact that the universe contains hotter structures at later times. The peak temperature at all redshifts falls within the warm-hot range, and by $z = 0$ it is up to $\sim 4 \times 10^6$ K. Note that this is close to the temperature of the excess diffuse emission seen by Wang & McCray (1993) in ROSAT data. Figure 5 also shows that the mass of the WHIM component is insensitive to our somewhat arbitrary choice of 10^5 K as the defining lower temperature. A choice of $10^{4.5}$ K (as in DHKW) or even $10^{5.5}$ K would not drastically affect our conclusions.

An analytic estimate of the evolution of the peak temperature can be obtained by considering the temperature of intergalactic gas shock heated on mildly nonlinear large-scale structure. If the length scale going nonlinear at a given epoch is $L_{\rm nl}$, and the perturbation collapses on a timescale t, the resulting sound speed behind the shock will be $\sim L_{\rm nl}/t$. Given that the perturbation has taken a Hubble time to collapse, $t \sim H^{-1}$, where H is the Hubble constant at time t. The resulting post-shock temperature is then (CO99)

$$T_{\rm nl} \propto c_{\rm nl}^2 = K(HL_{\rm nl})^2 \, , \qquad (2)$$

where K is a constant, at any given epoch. The value of $T_{\rm nl}$, with $K = 0.3$, is shown at each redshift plotted in Figure 5 by the arrows above each curve. This value of K produces roughly the correct peak temperature at $z = 0$, and as can be seen from Figure 5, it is a reasonable fit to the peak temperature at higher redshifts, though it becomes progressively more difficult to identify a peak. This value of K also produces the correct evolution of the globally averaged temperature in simulations C1 and C2, as shown in CO99. Thus the evolution of the temperature distribution of WHIM gas is consistent with the interpretation that it is heated by gravitationally-induced shocks on mildly nonlinear large-scale structure. Since there is a wide range in the properties of the collapsing structures and therefore infall velocities, there is also a wide range in gas temperatures.

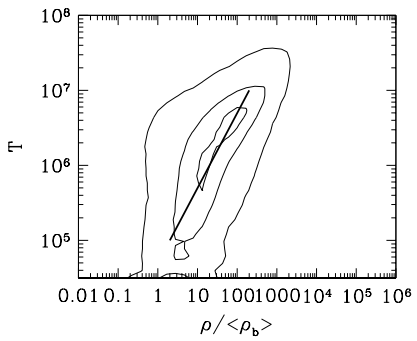

Figure 6: Contours in temperature and density for simulation D1 at $z = 0$, enclosing 10%, 50% and 90% of the baryons in the range shown. Density and temperature are correlated in the WHIM regime. Thick line indicates a scaling of $\rho/\bar{\rho}_b = T/10^{4.7}$ in the warm-hot temperature range.

The temperature and density of WHIM gas are correlated. Figure 6 shows a contour plot of mass within the warm-hot range, as a function of density and temperature, for the D1 model at $z = 0$. The contour levels enclose 10%, 50% and 90% of the mass in the temperature and density ranges shown in the plot. The thick line indicates an "equation of state" $\rho \propto T$ that provides a reasonable fit to gas in the range $10^5 < T < 10^7$ K. This relationship is different from that of diffuse gas, which typically has $\rho \propto T^{1.7}$, and the temperature-density relation of WHIM gas has much greater scatter. The higher temperature, different slope, and greater scatter all reflect the importance of shock heating as the dominant mechanism controlling the thermal properties of WHIM gas; the "equation of state" for diffuse gas, on the other hand, arises from the competition between photoionization and adiabatic cooling due to Hubble expansion (Hui & Gnedin 1997). Figure 6 also suggests that detecting WHIM gas in emission will be easier for gas that is at the highest end of the WHIM temperature range, since that gas will be both denser and hotter. However, the dominant portion of WHIM gas is at lower temperatures, which is perhaps most easily detected via absorption lines (Tripp, Savage & Jenkins 2000).

5. CONSTRAINTS FROM THE SOFT X-RAY BACKGROUND

Gas with temperatures in the range $10^5 < T < 10^7$ K will emit thermally in the soft X-ray band. The extragalactic soft X-ray foreground (SXRB) flux at 0.1-0.4 keV is roughly $\sim 20 - 35$ keV cm^{-2}s^{-1}sr^{-1}keV^{-1} (Warwick & Roberts 1998), though uncertainties are large because galactic coronal gas provides an increasing foreground to lower energies. At slightly higher energies ($\sim$ 1 keV), the XRB has further been resolved nearly completely ($\sim 80 - 90\%$) into point sources, mostly AGN (Mushotsky et al. 2000). Reasonable arguments then allow only a small contribution to the SXRB from diffuse gas, $\lesssim$ 4 keV cm^{-2}s^{-1}sr^{-1}keV^{-1} (Wu, Fabian & Nusser 1999, hereafter WFN). Such a limit, in principle, places constraints on the amount of gas in the universe at warm-hot temperatures.

These limits were explored in two independent papers using similar methodologies, WFN and Pen (1999). Both papers argue that the standard picture of hierarchical formation of virialized objects results in a predicted SXRB that exceeds the observed limits. They suggest that significant non-gravitational heating, typically ~ 1 keV per baryon, is required to unbind warm-hot gas from virialized objects in order to satisfy the SXRB constraints. In this section we discuss these constraints in the context of WHIM gas, and find that our simulations paint a very different picture for soft X-ray emission than the simple models assumed in those two papers. A full calculation of the SXRB from these simulations is a complicated undertaking (because of metallicity, bandpass, and numerical issues) that is beyond the scope of this paper. However, the physical properties of WHIM gas in the simulations are quite different from the properties assumed by WFN and Pen (1998), and we will show that scaling our results to theirs suggests that the observed SXRB flux does not rule out the WHIM predicted by these simulations. The essential difference is one of density. Both WFN and Pen (1998) base their calculations on a Press-Schecter (1974) analysis, which implicitly assumes that gas is in virialized objects with typical overdensity $\gtrsim 200$. However, most of the WHIM gas in the simulations is in lower-density filamentary structures rather than virialized objects, thus the SXRB emission is lower (cf. Figure 5).

We can quantify this difference in typical overdensity by considering the clumping factor of the emitting gas. If we define the clumping factor for gas component g as

$$C_g \equiv < \rho_g^2 > / < \rho_g >^2, \quad (3)$$

then the free-free emissivity from that component is

$$\epsilon_{\rm SXRB} \propto < \rho_g^2 T_g^{0.5} > \propto C_g \Omega_g^2 T_g^{0.5}, \quad (4)$$

where ρ_g, Ω_g, $T_g \approx 10^6$ K, and C_g are the density, mass fraction, temperature, and clumping factor of the gas emitting in soft X-rays. The flux $j_{\rm SXRB}$ of soft X-ray background is then the emissitivity multiplied by path length $\sim \frac{1}{3} c H^{-1}$. WFN argue, sensibly, that it is predominantly warm-hot gas ($10^5 < T < 10^7$ K) that is responsible for soft X-ray emission. This means the appropriate clumping factor C_g is that of *warm-hot* gas, $C_{\rm WHIM}$.

There are several ways to calculate $C_{\rm WHIM}$ in our simulations. One can directly calculate it from equation 3, which is the approach we use for our Eulerian simulations. For Lagrangian simulations, because each particle represents a different volume of gas, it becomes more numerically convenient to calculate $C_{\rm WHIM} \approx \xi_{\rm WHIM}(0)$, where $\xi_{\rm WHIM}(r)$ is the two-point correlation function of WHIM gas at radius r.

The resulting $C_{\rm WHIM}$ values for our simulations at $z = 0$ are listed in Table 1. All simulations show clumping factors in the range $\sim 30 - 400$. The smaller clumping factors in C1 and C2 arise directly because the WHIM gas is typically less dense in these models as compared to D1, D2, B1 and B2 due to greater supernova feedback in the diffuse IGM, as explained before.

Our clumping factors are significantly less than that used by Pen (1999), who adopts $C \gtrsim 900$ and argues $C \gtrsim 10^4$. The reason is that the clumping factor of Pen (1999) is actually that of *all* gas (assumed to trace the dark matter), not the warm-hot baryons. Such a clumping factor is dominated by the contribution from galaxies and other collapsed, virialized structures. This is not the appropriate clumping factor with which to calculate the soft

X-ray background, since as we have shown in the previous section, WHIM gas is typically at much lower overdensities than virialized structures. In Pen (1999), the clumping factor is strongly dependent on simulation resolution, because it is dominated by the highest overdensity objects. Amongst our simulations, a wide range of resolutions give barely an order of magnitude difference in clumping factor, since the WHIM gas is predominantly diffuse.

Pen (1999) determines that ~ 1 keV of non-gravitational heating would reduce his clumping factor to $C \lesssim 60$, which he argues is necessary to satisfy XRB constraints. However, this was derived assuming that all gas contributes to the SXRB (see his eq. 2), whereas in our simulations only $\sim 30\%$ of the baryons contribute to the SXRB (probably an even smaller fraction since the narrow range of SXRB energies arises from a narrower range of gas temperatures than $10^5 < T < 10^7$ K). From equation 4, we see that a reduction in Ω_g, the mean density of emitting gas, results in an increase in the maximum allowed clumping factor by $(\Omega_b/\Omega_{\rm WHIM})^2 \approx 10$. Thus his analytically-derived constraint translates to $C_{\rm WHIM} \lesssim 600$. Our clumping factors ($\lesssim 400$) are consistent with his analysis, despite the fact that WHIM gas in our simulations undergoes almost no non-gravitational heating.

WFN present a more detailed model from which we can crudely estimate our SXRB by comparison. They do not specifically use clumping factors to predict the SXRB in their model, but they perform a similar calculation to that of Pen (1999), based on a Press-Schecter analysis with an assumed halo profile. The Press-Schecter formalism makes two assumptions about how gas is distributed and heated in the universe: (1) All soft X-ray emitting gas is bound in virialized halos (namely, groups of galaxies); (2) Gas can only be heated by accretion onto a virialized halo, with the gas temperature set by the virial temperature of the halo. Unlike Pen (1999), they allow some gas to cool and therefore not emit in X-rays, but this is a small correction. In their model, the gas clumping factor is the clumping factor of *virialized* objects, since they are assuming that emitting gas solely resides in such objects.

Our simulations suggest that both Press-Schecter assumptions are strongly violated in the case of WHIM gas. First, only a small fraction of WHIM gas is bound in virialized halos; most is distributed much more diffusely. Second, in our simulations, intergalactic gas can be heated significantly by purely gravitational processes prior to being accreted onto a virialized object.

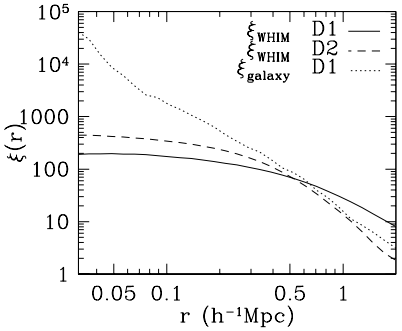

Figure 7: Two-point correlation functions for WHIM gas from simulation D1 (solid line) and D2 (dashed line), and for galaxies from simulation D1 (dotted line).

The two-point correlation function $\xi_{\rm WHIM}$ illustrates quite clearly that WHIM gas is not bound in virialized halos, and is instead associated with large-scale structure. Figure 7 shows $\xi_{\rm WHIM}$ for simulation D1 (solid line), D2 (dashed), as well as $\xi_{\rm galaxy}$ (dotted line) calculated from D1. $\xi_{\rm galaxy}$ is computed as the correlation function of all star particles in this simulation, where stars are formed slowly out of cold, dense gas and are seen to trace the galaxy population (see Katz, Weinberg & Hernquist 1996). At scales less than a few hundred kpc, $\xi_{\rm WHIM}$ flattens, indicating that WHIM gas does not cluster on scales smaller than those typical of large-scale structures. Conversely, the galaxy correlation function continues as approximately a power law in to the resolution limit of our simulation. The clumping factor of WHIM gas, $\xi_{\rm WHIM}(0)$, is well-defined since we can meaningfully extrapolate from our resolution limit to $r = 0$. This is not true for the clumping factor of galaxies, for which we may only set a lower limit (consistent with Pen 1999), $C_{\rm galaxy} \gtrsim 4 \times 10^4$.

We can crudely estimate the SXRB flux we would predict in comparison to that predicted by WFN by multiplying their predicted $j_{\rm SXRB}$ by $C_{\rm WHIM}/C_{\rm galaxy}$. This corrects for the fact that they use virialized objects (which we take as galaxies) instead of the true diffuse WHIM responsible for SXRB emission. Thus we would roughly predict a SXRB flux that is two orders of magnitude lower than that predicted by WFN. Examining their Figure 2 or 3 shows that such a reduction in $j_{\rm SXRB}$ makes the SXRB contribution from warm-hot gas consistent with observational limits.

In summary, the discrepancies in the predicted soft XRB versus previous studies arise from their use of a Press-Schecter analysis, or an equivalent method that implicitly places emitting gas into virialized objects, in order to study an intergalactic component of baryons that is inherently much more diffuse. These methods do not allow for gravitational shock heating in unbound objects such as filaments, thus they are forced to postulate significant non-gravitational heating to make the emitting gas more diffuse. In our scenario, most WHIM gas has never fallen into virialized objects, though it is still heated (almost) purely via gravitational processes. Scaling previous analyses by the typical overdensities found in our simulations suggests that the properties of the predicted WHIM are consistent with SXRB constraints. However, these scaling arguments are approximate at best, and not enough to guarantee consistency. More accurate calculations of X-ray emission from these simulations are certainly warranted and may yield interesting constraints on the WHIM component; these issues will be addressed in detail in separate papers (Fardal et al., in preparation; Phillips et al., in preparation).

6. SUMMARY

We study the warm-hot intergalactic medium (WHIM), defined as all the gas in the universe with temperature $10^5 < T < 10^7$ K, in six cosmological hydrodynamic simulations with widely varying spatial resolutions, volumes, code algorithms, and input physics. In each simulation, the WHIM contains $\approx 30 - 40\%$ of all baryons in the present-day universe. As a rule of thumb, our simulations predict that the fractions of baryons in the warm-

hot phase, the diffuse phase, and gravitationally bound systems are roughly comparable at the present epoch.

The WHIM is comprised primarily of gas at moderate overdensities, with a median overdensity $\sim 10-30$, and is predominantly an intergalactic component. It is shock-heated by accretion onto non-equilibrium filamentary large-scale structures, with possibly a small energy contribution from non-gravitational processes such as supernova feedback. Despite being heated primarily by gravitational processes, WHIM gas in our simulations is consistent with constraints from the soft X-ray background. The clumping factors of WHIM gas in our simulations range from $\sim 30-400$, which are far below that of virialized objects ($\gtrsim 10^4$) that some studies assume are the sources of soft XRB photons.

Different simulations give somewhat different fractions of WHIM gas at the present epoch, though the fraction is significant in all simulations. We argue that the differences are primarily attributable to resolution effects, specifically manifested in the distribution of supernova feedback energy in different simulations. In high spatial resolution simulations, the added heat remains in dense regions and radiates away almost immediately, whereas in lower spatial resolution simulations a significant fraction of heat ends up in diffuse intergalactic gas where it cannot radiate away. Still, the differences in present-day WHIM fraction are not large between these two somewhat extreme cases for feedback. Radiative cooling plays a minor role in the evolution of warm-hot gas because it is mostly at low densities, and is too diffuse to self-gravitate and self-shield into mini-halos. Other physical effects such as star formation, photoionization, and cosmic variance do not produce significant differences in the amount or properties of warm-hot gas in our simulations.

Since the exact predicted fraction of WHIM gas is as yet sensitive to simulation details, it would be greatly beneficial to place observational constraints on this component. As mentioned before, this is a challenging task. Still, there are tantalizing hints of detections of WHIM gas. Wang & McCray (1993) found an excess emission component in ROSAT data around $T \sim 2\times10^6$ K, which may be arising from this diffuse component. Soltan et al. (1996) detected an auto-correlation signature between the soft X-ray background and galaxies, as would be expected if warm-hot gas was distributed in large-scale structures. Even more exciting is a possible direct detection of diffuse soft X-ray emission associated with a filament of galaxies, by Scharf et al. (2000). Somewhat stronger evidence comes from a census of O VI absorbers at redshifts $0.14 \lesssim z \lesssim 0.27$ (Tripp, Savage & Jenkins 2000; Tripp & Savage 2000), which together with conservative ionization corrections and metallicities implies $\Omega_{\rm WHIM} \gtrsim 0.003^{+0.004}_{-0.002} h_{75}^{-1}$, or $\Omega_{\rm WHIM}/\Omega_b \gtrsim 10\%$ at the present epoch. However, some of these O VI absorbers may be photoionized, arising in cooler, low-density intergalactic gas at $T \sim 10^4$ K.

WHIM gas emission may be easiest to detect around high density regions such as clusters because that is where the density and temperature are highest within the WHIM range (cf. Figure 6), but this is *not* where the majority of WHIM gas is located. For instance, high-resolution Chandra spectra of regions between clusters that are free of bright sources may provide a detectable signal (Phillips et al., in preparation), and observations from XMM could possibly image filaments of warm-hot gas directly (Pierre, Bryan & Gastaud 2000). Our simulations, however, predict the majority of WHIM gas is far away from galaxies and clusters, residing in the diffuse IGM. A promising avenue to detect this more typical WHIM gas is via absorption, as continuing observations with STIS aboard Hubble will detect many more O VI absorbers. Future X-ray satellites may be able to detect higher ionization absorbers such as O VII and O VIII that may also trace WHIM gas (Hellsten, Gnedin & Miralda-Escudé 1998). The detection of this component is a key observational challenge, as the warm-hot intergalactic medium is rapidly become an integral part of our understanding of the evolution of baryons in the universe.

We thank Jeff Gardner, Ed Jenkins, Richard Mushotsky, Arielle Phillips, Jim Peebles and Todd Tripp for helpful discussions. RD is supported by NASA ATP grant NAG5-7066. RC and JPO are supported by NSF grants AST-9803137 and ASC-9740300. Support for GLB was provided by NASA through Hubble Fellowship grant HF-01104.01-98A from the Space Telescope Science Institute, which is operated by the Association of Universities for Research in Astronomy, Inc., under NASA contract NAS5-26555. This work was supported by NASA Astrophysical Theory Grants NAG5-3922, NAG5-3820, and NAG5-3111, by NASA Long-Term Space Astrophysics Grant NAG5-3525, and by the NSF under grants ASC93-18185, ACI96-19019, and AST-9802568. Some of the simulations were performed at the San Diego Supercomputer Center. We also thank NCSA for use of their computing facilities.

REFERENCES

Bahcall, N., Ostriker, J. P., Perlmutter, S., & Steinhardt, P. J. 1999, Science, 284, 1481
Bryan, G. L. 1999, "Computing in Science & Engineering", Vol. 1, No. 2, p. 46
Cen, R., Miralda-Escudé, J., Ostriker, J. P., & Rauch, M. 1994, ApJ, 427, L9
Cen, R. & Ostriker, J. P. 1999, ApJ, 519, L109 [CO99]
Davé, R., Dubinski, J., & Hernquist, L. 1997, NewAst, 2, 71
Davé, R., Hernquist, L., Katz, N., & Weinberg, D. H. 1999, ApJ, 511, 521 [DHKW]
Efstathiou, G. 2000, MNRAS, submitted, astro-ph/0002245
Fukugita, M., Hogan, C. J., & Peebles, P. J. E. 1998, ApJ, 503, 518
Hellsten, U., Gnedin, N., & Miralda-Escudé, J. 1998, ApJ, 506, 56
Hernquist, L., Katz, N., Weinberg, D.H., & Miralda-Escudé, J. 1996, ApJ, 457, L51
Hogan, C. J. 1999, proc. "Inner Space/Outer Space II: the David Schramm Memorial Symposium", astro-ph/9912107
Hui, L. & Gnedin, N. 1997, MNRAS, 292, 27
Kang, H., Ostriker, J. P., Cen, R., Ryu, D., Hernquist, L., Evrard, A. E., Bryan, G. L., & Norman, M. L. 1994, ApJ, 430, 83
Katz, N., Weinberg D. H., & Hernquist, L. 1996, ApJS, 105, 19
Mac Low, M.-M. 2000, invited review for Stars, Gas, and Dust in Galaxies (eds. D. Alloin, K. Olsen, and G. Galaz), astro-ph/0006322
Miralda-Escudé, J., Cen, R., Ostriker, J. P., & Rauch, M. 1996, ApJ, 471, 582
Mushotsky, R. F., Cowie, L. L., Barger, A. J., & Arnaud, K. A. 2000, Nature, 404, 459
Pen, U.-L. 1999, ApJ, 510, 1L
Press, W. H. & Schecter, P. 1974, ApJ, 187, 425
Pierre, M., Bryan, G., & Gastaud, R. 2000, A&A, 356, 403

Rauch, M., Miralda-Escudé, J., Sargent, W. L. W., Barlow, T. A.,Hernquist, L., Weinberg D. H., Katz, N., Cen, R., Ostriker, J. P. 1997, ApJ, 489, 7
Rauch, M. 1998, ARA&A, 36, 267.
Ryu, D., Ostriker, J. P., Kang, H., & Cen, R. 1993, ApJ, 414, 1
Scharf, C., Donahue, M., Voit, G. M., Rosati, P., & Postman, M. 2000, ApJ, 528, L73
Soltan, A. M., Hasinger, G., Egger, R., Snowden, S., & Truemper, J. 1996, A&A, 305, 17
Tripp, T. M., Savage, B. D. 2000, ApJ, 542, in press, astro-ph/0004135
Tripp, T. M., Savage, B. D., & Jenkins, E. B. 2000, ApJ, 534, L1
Tytler, D., Fan, X.M., & Burles, S. 1996, Nature, 381, 207
Wang, Q. D. & McCray, R. 1993, ApJ, 409, L37
Warwick, R. S. & Roberts, T. P. 1998, Astronomische Nachrichten, 319, 59.
Wu, K. K. S., Fabian, A. C., & Nulsen, P. E. J. 1999, MNRAS, in press [WFN]
Zhang, Y., Anninos, P., & Norman, M.L. 1995, ApJ, 453, L57